Elsevier Editorial System(tm) for Ceramics International
Manuscript Draft

Manuscript Number: CERI-D-14-04126R1

Title: Nanoindentation and fracture toughness of nanostructured zirconia/multi-walled carbon nanotube composites

Article Type: Full Length Article

Keywords: Ceramic-matrix composites (CMCs); Carbon nanotubes; Mechanical properties; Fracture toughness; short pulse laser machining.

Corresponding Author: Ms. Latifa Melk, Ph.D.

Corresponding Author's Institution: Universitat Politècnica de Catalunya (UPC)

First Author: Latifa Melk, Ph.D.

Order of Authors: Latifa Melk, Ph.D.; Joan Josep Roa Rovira; Fernando García-Marro; Marta-Lena Antti; Ben Milsom; Michael Reece; Marc Anglada

Abstract: Multi-walled carbon nanotubes (MWCNTs)/3 mol% yttria-doped tetragonal zirconia (3Y-TZP) composites were produced using spark plasma sintering (SPS) with MWCNT content ranging within 0-2 wt%. In the present paper, it was shown that the addition of MWCNTs results in a refinement of the composites microstructure. Moreover, nanoindentation tests were performed in order to monitor the change in elastic modulus and hardness with MWCNT content and it was found that both properties decrease with the addition of MWCNT content. A novel method was used to measure the true fracture toughness of the composites by producing a shallow surface sharp notch machined by ultra-short pulsed laser ablation on the surface of beam specimens. The true fracture toughness obtained on this laser machined single edge V-notch beam (SEVNB) specimens tested in four point bending was compared to the indentation fracture toughness measured using a Vickers indenter. It was found that the indentation fracture toughness increases with increasing MWCNT content, while the true fracture toughness determined with SEVNB was practically independent of the composition. Finally, it was concluded that the increase in the resistance to indentation cracking of the composites with respect to 3Y-TZP matrix cannot be associated to higher true fracture toughness. The results were discussed in terms of transformation toughening, damage induced in front of the notch tip, microstructure of the composites, and fracture toughness of 3Y-TZP.

We thank the referees for their comments which have been helpful to increase the quality of the manuscript. Please find below the answers to the referee comments. We have also made slight changes in the manuscript in red colour.

Response on Referee comments:

1) **Beginning of section 3.1 describes density of the prepared materials. How big is the porosity? Also, it would be good if the pores were characterized in terms of size and shape, and possibly locations (I guess they would be connected to the MWCNTs). This might be of a consequence for the crack propagation.**

The drop in density of the composites seen in Table 1 is related to the presence of porosity connected to the CNT agglomerates.
Fig. 1 shows the fracture surface of the composite with 2 wt% CNT content where some pores related to the clusters of MWCNTs could be observed.
In order to measure with better accuracy the grain size of the composites and to see clearly the grain boundaries, the composites were etched by a heat treatment at high temperature in air and the locations of the burned out CNTs were revealed. See fig. 2 of the manuscript. (See changes in red colour in the manuscript)

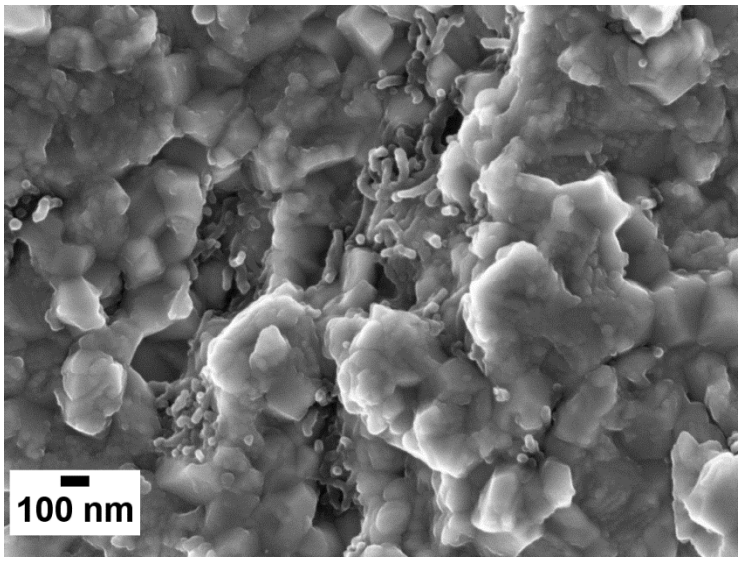

Fig. 1 Fracture surface showing the presence of porosity in the composite with 2 wt% CNT content.

2) **Section 3.2 and Fig.3 describe the nanoindentation results. For most of the materials the values stabilize for depths <100 nm, it is only for the one with 0.5 % CNTs that they increase very slowly. What is the reason? Is it some real problem of the material or the tip, or it can be just because of some really bad measurement which should have been eliminated from the statistics? The scatters are not too large, so it seems it could be an artifact coming from tip geometry. Could the authors comment on that?**

As the reviewer comments, it is true that the scatters for the 0.5% wt. CNT is not too large, however, the hardness trend does not stabilize until 1000 nm of displacement into surface as it can clearly be observed in Fig. 3a. This phenomenon cannot be attributed to an artifact coming from the tip geometry because the indenter tip was calibrated using fused silica and all the samples were tested in the same day under the same experimental conditions. Furthermore, all the different tests performed for this condition presented the same trend. Therefore, the behavior of 0.5 wt% CNT could be attributed to a real problem of the material. However, this does not change the trend of the effect of CNT on 3Y-TZP presented in the manuscript.
No additional changes have been introduced in the reviewed manuscript

3) P**age 14, 1st paragraph - the increase in contact damage resistance measured by indentation is attributed to the weak interfacial bonding between the matrix and CNTs. It is difficult to judge, since no photographs of crack lines and no information on porosity are presented. Is it possible that the cracks are arrested by voids or microcracks?**

There are slight differences in morphology of the crack path (see figure below), but we understand that they are small and do not contribute significantly to the indentation fracture toughness. We rather associate the enhanced contact-damage resistance related to a reduction in the driving force for crack growth related to change in plastic deformation behaviour below the indentation. The intense confined-shear under Vickers indentation in the presence of shear-deformable MWCNTs in the small agglomerates increases irreversible deformation by this mechanism as well as by compaction of porosity below the indenter instead of by plastic deformation. The series of indentation fracture toughness of the literature are based on the assumption of plastic deformation below the indenter but here they are not fully applicable: as the CNT concentration increases there are additional mechanisms to change shape below the indenter (shear of bundles of nanotubes and porosity compaction) which induce a smaller driving force for crack growth.
(See changes in red colour in the manuscript).

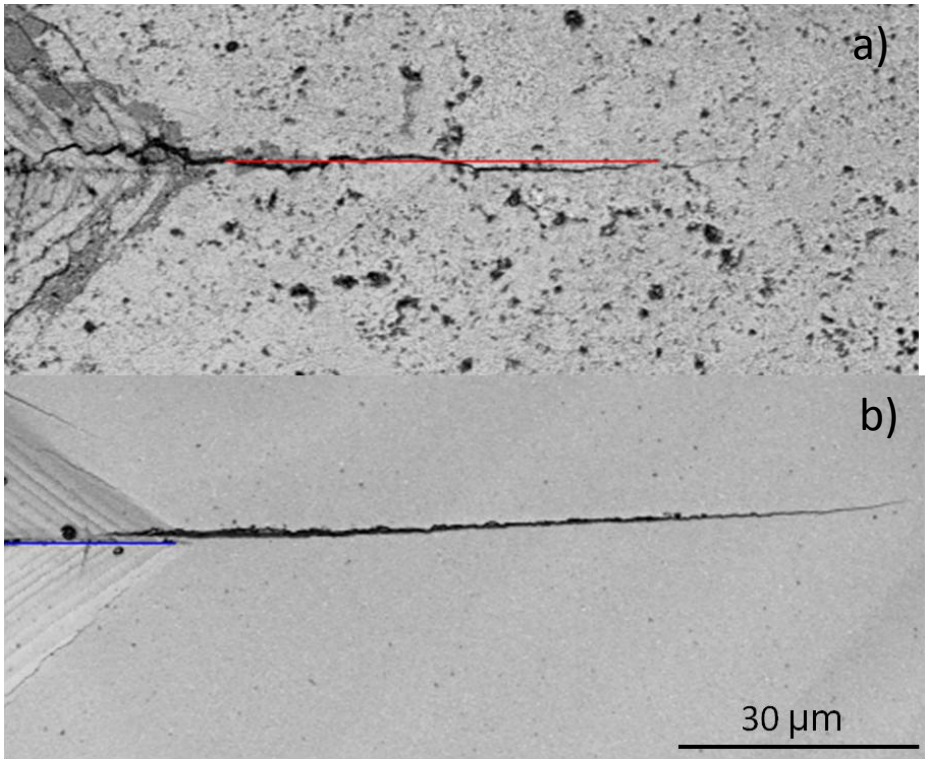

Fig. Indentation cracks in the composites with **a)** 2 wt% CNT and with **b)** 0% wt% CNT (Red and blue lines were used to measure crack length and diagonals of residual imprint respectively). This picture is not incorporated in the manuscript

4) Page 14, section "Damage" claims that no slip lines were observed (Fig. 7). The size of the indents is simply too big, resolution of the images in Fig.7 and quality of the surfaces is completely inadequate to observe the slip lines. While I agree that it is likely that the dominant process is the (nano) grain sliding and not their plastic deformation or transformation, the evidence as presented is insufficient.

We completely agree with this comment. The resolution of this image is completely inadequate. This was a mistake by our part for which we apologize. We have modified the text like that: No fracture events like radial cracks at the corners of the imprints were detected. (See changes in red colour in the manuscript).

5) It would be interesting to see the morphology of the laser machined notch in cross section. Can the authors provide such a picture?

We have incorporated in the manuscript a new figure (Fig. 5) in which the notch for the composite with 0 wt% CNT content is presented.
In order to get a close overview of the notch, the top surface of the notch (surface on which the notch was induced) was grinded step by step, then polished till approximately the mid depth of the notch is reached. The damage zone below the notch is hardly seen before

fracture. However, the damage could easily be detected after fracture. See fig. 6 of the manuscript. (See changes in red color in manuscript).

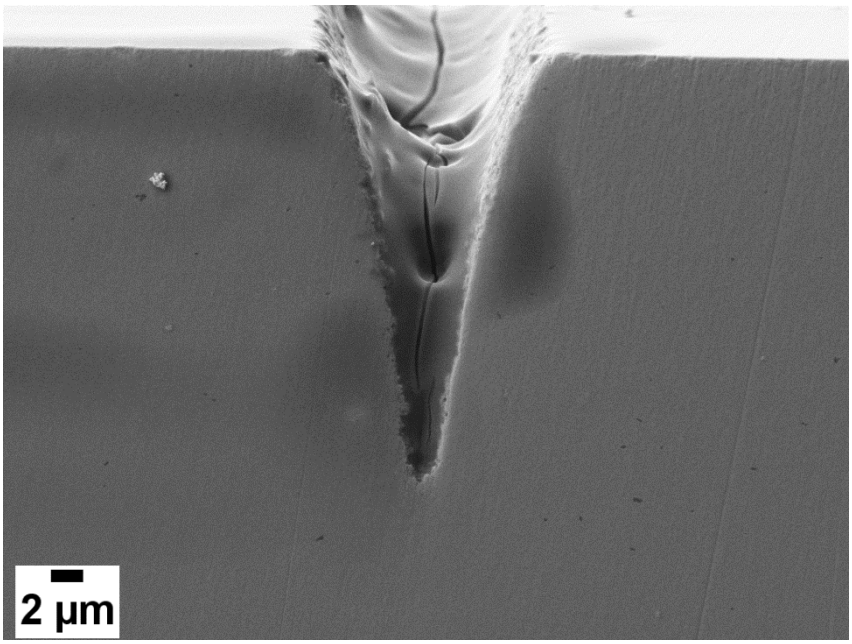

Fig. 5 View of the morphology of the notch induced by UPLA on the specimen with 0 wt% CNT content.

Nanoindentation and fracture toughness of nanostructured zirconia/multi-walled carbon nanotube composites

Latifa Melk [‡,§,$] , Joan J. Roa Rovira[‡], Fernando García-Marro[‡], Marta-Lena Antti[§], Ben Milsom[*,¶], Michael J. Reece[*,¶], and Marc Anglada[‡†]

[‡]*Department of Materials Science and Engineering, Universitat Politècnica de Catalunya, Barcelona, 08028, Spain*

[§]*Department of Engineering Sciences and Mathematics, Luleå University of Technology, Luleå, Sweden*

[*]*Department of Materials, Queen Mary College, University of London, London E1 4NS, UK*

[¶]*Nanoforce Technology Limited and School of Engineering and Materials Science, Queen Mary, University of London, London E1 4NS, UK.*

[$]Corresponding author at: Department of Materials Science and Engineering/ETSEIB
Diagonal 647. 08028-Barcelona
Tel. +34 934016701
Fax. +34 934016706
E-mail: melk.latifa@gmail.com

Abstract

Multi-walled carbon nanotubes (MWCNTs)/3 mol% yttria-doped tetragonal zirconia (3Y-TZP) composites were produced using spark plasma sintering (SPS) with MWCNT content ranging within 0-2 wt%. In the present paper, it was shown that the addition of MWCNTs results in a refinement of the composites microstructure. Moreover, nanoindentation tests were performed in order to monitor the change in elastic modulus and hardness with MWCNT content and it was found that both properties decrease with the addition of MWCNT content. A novel method was used to measure the true fracture toughness of the composites by producing a shallow surface sharp notch machined by ultra-short pulsed laser ablation on the surface of beam specimens. The true fracture toughness obtained on this laser machined single edge V-notch beam (SEVNB) specimens tested in four point bending was compared to the indentation fracture toughness measured using a Vickers indenter. It was found that the indentation fracture toughness increases with increasing MWCNT content, while the true fracture toughness determined with SEVNB was practically independent of the composition. Finally, it was concluded that the increase in the resistance to indentation cracking of the composites with respect to 3Y-TZP matrix cannot be associated to higher true fracture toughness. The results were discussed in terms of transformation toughening, damage induced in front of the notch tip, microstructure of the composites, and fracture toughness of 3Y-TZP.

Keywords: Ceramic-matrix composites (CMCs); Carbon nanotubes; Mechanical properties; Fracture toughness; short pulse laser machining.

1. Introduction

In the last decades there has been growing interest in developing ceramic materials with high fracture toughness (K_{Ic}) and strength for structural applications. In the specific case of 3 mol% yttria-doped tetragonal zirconia (3Y-TZP), K_{Ic} can be increased by promoting phase transformation from tetragonal (t) to monoclinic (m) phase in front of a propagating crack tip (so called transformation toughening) [1]. However, as stronger is the tendency for stress induced transformation, as higher is the risk for premature spontaneous t-m transformation on the external surface in contact with moisture in the environment. This effect is referred to as hydrothermal degradation or low temperature degradation (LTD) and it is accompanied by surface microcracking. This phenomenon is the main drawback for the wider use of 3Y-TZP. It is more severe at higher temperatures, for larger grain sizes, and under the presence of tensile residual stress or low concentrations of yttria [1].

The resistance to LTD can be strongly increased by reducing the grain size into the nanoscale. However, this will reduce the transformation toughening capability, so that the fracture toughness will diminish [2]. One strategy to counteract LTD is the incorporation of a second phase as a toughening mechanism in the form of particles, grains, whiskers or fibres into the nano-grain zirconia matrix.

Recent investigations have been focused on the addition of carbon nanotubes (CNTs) as reinforcements into a ceramic matrix because of their high aspect ratio and outstanding mechanical properties [3]. Moreover, it was reported that the addition of CNT to TZP-based composites improves the fracture toughness without affecting the resistance to LTD [1].

On the other hand, there is still a debate about the efficiency of CNTs in the mechanical properties of the ceramic matrix nanocomposites. Zhan et al. [4] reported an important improvement in indentation K_{IC} (K_{IC} ~9.7 MPa.m$^{1/2}$) with addition of 10 vol.% SWNTs to Al_2O_3 matrix, but Wang et al. [5] found a much smaller improvement (only 3 %) when K_{IC} was measured by the single edge V-notch beam (SEVNB) method on the same nanocomposites. A key observation made on these alumina composites is that they can be more contact-damage resistant than alumina, as it was shown by the lack of crack formation during indentation tests, and, in the same time, they were brittle as dense Al_2O_3 with low K_{Ic} measured by the SEVNB method [5]. Therefore, it was concluded that for the alumina composites studied, a high tolerance to indentation loading does not necessarily represent an increase in K_{Ic}.

Some studies about the incorporation of multi-walled carbon nanotubes (MWCNTs) to 3Y-TZP matrix reported an increase in indentation K_{Ic} using different techniques for the processing of 3Y-TZP/CNT composites [6–9]. Values up to 13 MPa.m$^{1/2}$ have been reported for the addition of 1 wt.% SWNTs [10]. Other authors have found that the increase in indentation K_{Ic} only occurs for the addition of relatively small CNTs content: 0.5 wt.% ([11,12]), 1.0 wt.% [11]. However, an increase of K_{Ic} was also reported for the addition of 4 wt% of functionalized CNTs [12]. While, a decrease in indentation K_{Ic} was usually observed for concentrations higher than 2 wt% CNT [11–15] and explained by the poor dispersion of CNTs and the weak bonding between CNTs and zirconia matrix. Moreover, a decrease in K_{Ic} was reported in 1.07 wt% CNF/CNT [16,17] as well as by adding a small fraction of ~0.69 wt.% carbon nanofibers (CNF) [18].

Regarding the influence of CNT on the Vickers hardness to 3Y-TZP, most of the studies have concluded that with the addition of either small CNT content (~ 0.5%)

([6,7,9]) or above relatively high content, the hardness decreases with the addition of CNT or CNF to monolithic zirconia [8,10,11,14–18]. One exception is the work of Mazaheri et al. [7], who reported a slight increase for the addition of 5 wt.% MWCNT.

The reason of the disparity of K_{Ic} results in the literature, mentioned in the previous part, is probably related to the use of indentation method. It was reported [19] that the indentation method can give unreliable results as shown before for SWNT-Al_2O_3 composites [5]. Thus, alternative methods to indentation are necessary to be used to measure the true K_{Ic}.

Single edge V-notch beam method has been used as a reliable method to measure $K_{IC.}$ Fracture toughness values of 8.1 MPa√m for 5 wt% 3Y-TZP/CNT have been reported [7,20]. A critical issue with this method is the sharpness of the notch tip. It is well known that notches induce more moderate stress fields than cracks and this may lead to an overestimation of K_{Ic}, However, since sharp microcracks are produced in front of the notch during machining, the notch tip radius should be smaller than the size of machining-induced defects in order that the SEVNB method can be applied for the determination of K_{Ic} [21]. As the length of these microcracks are proportional to the grain size, they can be long enough in coarse grain structures, but in fine grain ceramics this condition is difficult to fulfil even by sharpening the notch tip with a razor blade impregnated with diamond paste. This point was investigated experimentally in a European round robin where it was concluded that the radius of the starting notch in 3Y-TZP (grain size ~0.4 μm) should be less than about 1 μm [22]. Therefore, in both 3Y-TZP and 3Y-TZP/CNT processed by spark plasma sintering (SPS) with grain size even much smaller than conventionally processed 3Y-TZP, the required notch tip radius is too small to be introduced by honing. Recently, the effect of notch tip radius on K_{Ic}

has been studied by Fischer et *al*.[23] in 3Y-TZP of 400 nm grain size. They obtained large values of K_{Ic} ranging from 5.9 to 13.6 MPam$^{1/2}$ for notch root radii between 18 and 167 μm.

The purpose of this paper is to study the influence of MWCNT content on the mechanical properties of 3Y-TZP and to calculate the true K_{Ic} of 3Y-TZP matrix and 3Y-TZP/CNT composites, both produced by SPS, by applying a novel method based on inducing a shallow surface sharp notch machined by ultra-short pulsed laser ablation (UPLA) and finally to compare the results with those obtained by Vickers indentation on the same materials.

2. Experimental procedure

2.1 Processing of nanocomposites

Composites with four different amounts of MWCNTs (0, 0.5, 1 and 2 wt.-%) were prepared. The starting materials were high pure (99.9 %) zirconia powder (TZ-3YSB-E, Tosoh, Japan) with crystalline size of 36 nm and MWCNTs (Graphistrength C100, Arkema, France) sintered by SPS (SPS FCT HP D25I, FCT System Gmβh, Germany). The details of the processing and preparation of samples are described elsewhere [24]. All samples were sintered at a temperature of 1350 °C with a dwell time of 5 min, with heating and cooling rates of 100 °C/min. A pressure of 50 MPa was maintained during the sintering cycle. The final samples were ceramic discs with 3 mm thickness and 40 mm diameter. The discs were polished using series of diamond suspensions from 30 to 3 μm then with colloidal silica. Finally the discs were cut into bar (4 mm x 2.5 mm x 40 mm) specimens for mechanical testing. The cut faces were ground and polished.

Some of the polished samples were thermally etched at 1100 °C during 1 hour in order to reveal the microstructure. The average grain size was determined using the line intercept method on scanning electron microscopy (SEM) images and the density was determined by the Archimedes method**.**

2.2 Mechanical properties

The response to sharp contact loading was examined by indentation fracture testing method. The specimen's surface was indented by a Vickers indenter under 1 kg (9.81 N) load and the Meyer hardness (*H*) and the indentation K_{Ic} were determined. Taking into account the Palmqvist morphology of the indentation cracks, the expression proposed by Niihara et *al.* [25] for Palmqvist cracks is the most appropriate for determining the indentation K_{Ic}. However, since in the literature the equation of Anstis *et al*. [26] for indentation K_{Ic} of median radial cracks is often employed independently of the shape of the cracks, it will be used in this study in order to compare the present results with other published results.

As the grain size of the composites tested in this study is in the range ~148-174 nm, a very sharp notch is needed in order to ensure that microcracks left in front of the notch tip are larger than the notch tip radius [21,27]. A novel method has been used for measuring K_{Ic} based on introducing a sharp shallow surface notch by UPLA on the surface of prismatic bars which was parallel to the original discs and determining K_{Ic} from the strength in four point bending.

The femtolaser system used to produce the notch was a commercial Ti: Sapphire oscillator (Tsunami, Spectra Physics) and a regenerative amplifier system (Spitfire, Spectra Physics) based on chirped pulsed amplification. The femtolaser delivered 120 fs linearly polarized pulses at 795 nm with a repetition rate of 1 kHz. The pulse energy

used was 5 mJ and the focusing system was an achromatic doublet lens with 50 mm focal length. The samples were placed on a XYZ motorized stage and moved along one of the horizontal axis with a scanning speed of 50 μm/s. Four passes were needed to achieve the desired notch depth (~ 24 μm).

The stress intensity factor, K_I, was obtained by using the following expressions proposed by Munz and Fett [28]:

$$K_I = \frac{3F(S_1 - S_2)}{2BW^2} Y\sqrt{a} \qquad (1)$$

$$Y = \frac{1.1215\sqrt{\pi}}{\beta^{3/2}}\left[\frac{5}{8} - \frac{5}{12}\alpha + \frac{1}{8}\alpha^2\beta^6 + \frac{3}{8}\exp(-\frac{6.1342\alpha}{\beta})\right] \qquad (2)$$

where S_1 and S_2 are the outer and inner spans respectively, B is the thickness, W the width, F the applied load, a is the crack length, which is taken as the depth of the notch plus the small damage region in front of the notch, $\alpha = a/W$ and $\beta = 1-\alpha$. The tests were performed for 0, 0.5 and 2 wt% CNT. Additional tests were carried out in standard 3Y-TZP with larger grain size (~330 nm). Finally, the notched bar specimens (4 mm x 2.5 mm x 40 mm) were tested in a four point bending test device (DEBEN, Microtest, UK) in air with spans of 30/12 mm. The average stress rate was 2.4 MPa/s. Three specimens were used for each composition.

The method used in this study has recently been applied to conventionally sintered 3Y-TZP (330 nm grain size) [29] and the results for K_{Ic} were found to be similar to values determined by other methods using sharp starting cracks.

Nanoindentation tests were performed using a Nanoindenter XP from MTS~~Agilent Technologies~~ equipped with continuous stiffness measurements (harmonic displacement 2 nm and frequency of 45 Hz), using a pyramidal Berkovich diamond indenter. The strain rate was held constant at 0.05 s^{-1}. The nanoindentation curves were ~~analyzed~~analysed using the Oliver and Pharr method [30] in order to measure the nanoindentation hardness (H_{Berk}) and the elastic modulus (E_{Berk}) as a function of the penetration depth for each composition where H_{Berk} was defined as the ratio of load and contact area at maximum load. The indenter shape was carefully calibrated for true penetration depths as small as 50 nm by indenting fused silica samples of well-known Young's modulus (72 GPa). The indents were organized in a regularly spaced array of 25 indentations (5 by 5) at a maximum penetration depth of 2000 nm or until reaching the maximum applied load, 650 mN. Each indentation was performed with a spacing distance of 50 μm in order to avoid any overlapping effect.

2.3 Damage

The surface damage associated with residual nanoindentation imprints was visualized by atomic force microscopy (AFM, Dimension D3100 from Bruker), in tapping mode. All the images were processed with the WSxM software [31].

The subsurface damage induced during the nanoindentation tests as well as in front of the notch tip by UPLA were characterized using a dual beam Focused Ion Beam (FIB) /SEM Microscope (Zeiss Neon 40) and the fracture surfaces were characterized by field emission scanning electron microscope (SEM) (JSM-7001F, JEOL, Japan). A thin platinum layer was deposited on the sample prior to FIB machining in order to

minimize ion-beam damage. A Ga^+ ion source was used to mill the surface at a voltage of 30 kV. The final polishing of the cross-sections was performed at 10 pA.

3. Results and discussion

3.1 Processing of nanocomposites

The measured bulk densities are given in **Table 1** for the different composites where it can be seen that they drop from 99.4% for 3Y-TZP to 97.4% for the addition of 2 wt% CNT. For a given composition, the theoretical density (TD) was calculated according to the rule of mixtures. The zirconia TD was taken as 6.1 $g \cdot cm^{-3}$ and that of MWCNTs as 1.8 $g \cdot cm^{-3}$ since their exact density was not known and it depends of purity, number of walls and external diameter of CNTs [32]. The drop in density of the composites seen in Table 1 is related to the presence of porosity connected to the CNT agglomerates.

Fig. 1 shows the fracture surface of the composite with 2 wt% CNT content where some pores related to the clusters of MWCNTs could be observed. Moreover, the low density reported in this study is a common observation of practically all studies on 3Y-TZP/CNT composites [6–10] [14–18].

Fig. 21 shows the fracture surfaces of the sintered nanocomposites for all studied compositions. The carbon nanotubes are well dispersed in the composite (blue arrows) with the addition of 0.5 wt% MWCNTs but increasingly agglomerated with the increase of MWCNT content.

Fig. 32 Sshows the final microstructure of the SPSed composites after etching at high temperature in air. As MWCNT content increases, the microstructure reveals smaller grain size. A refinement of the grain size was observed from 174 to 148 nm for

0 up to 2 wt% CNT respectively (see **Table 1**). The decrease of grain size with adding MWCNTs content has been attributed to the presence of MWCNTs in grain boundaries which slows [9] or hinders the grain growth of zirconia grains [7].

3.2 Hardness and elastic modulus

Fig. 43 shows the Berkovich hardness and the elastic modulus of all composites in terms of penetration depth. It is clearly seen that the values are stabilised for penetration depth larger than 400 nm, while for lower penetration depths, these properties are affected by surface defects and roughness. Moreover, both H_{Berk} and E_{Berk} of all composites are smaller than for monolithic 3Y-TZP (see **Table 1**). On the other hand, the Meyer hardness of 3Y-TZP/CNT diminishes in a similar way to H_{Berk}, but with less scatter (see **Table 1**). Therefore, the trend is the same whether a small or relatively large surface area is tested.

Since the ratio $(E_{Berk}/H)^{1/2}$ practically does not change with MWCNT content and the length of the indentation cracks is shorter with increasing MWCNT amount, the indentation K_{Ic} increases (see **Table 1**). The value of K_{Ic} depends on whether the equation of Anstis *et al*. [26] or Niihara *et al.* [25] is used. Values in the range of 3.5–5.0 MPam$^{1/2}$ were found using Anstis *et al*. [26] (see **Ttable 1**), while the values were about 20–% higher if K_{Ic} was calculated using the equation of Niihara *et al.* [25] Therefore, it was concluded that the indentation K_{Ic} increases for the compositions studied independently of the equation used.

With respect to the 3Y-TZP matrix, the observed contribution of 0.5 wt% MWCNT to the indentation K_{Ic}, is in a good agreement with similar composition investigated by Mazaheri *et al*. [7]. In the same direction, Ukai *et al*. [13] showed that the addition of 0.5 wt% CNTs improves indentation K_{Ic} in about 0.5 MPam$^{1/2}$, similar to the present

results. However, our absolute values of indentation K_{Ic} are noticeably smaller even for the starting 3Y-TZP matrix.

3.3 True fracture toughness

Fig. 54 shows the morphology of the notch induced by UPLA in the composite with 0 wt% CNT content.

In order to get a close overview of the notch, the top surface of the notch (surface on which the notch was induced) was grinded step by step, then polished till approximately the mid depth is reached. The damage zone below the notch is hardly seen before fracture. However, the damage could easily be detected after fracture. See Fig. 6.

Fig. 6 shows the fracture surface of the notched in four point bending specimens for 0, 0.5 and 2 wt% MWCNT, where three different regions are well differentiated. The first one (region A), at the top, corresponds to the notch, region B has a length of about ~ 24 μm with a different fracture surface appearance, and region C at the bottom has the usual common surface fracture appearance of zirconia. The transition between regions B and C is clearly defined by a relatively sharp straight border normal to the crack advance (see **Fig. 75**).

The extension of region B increases slightly with the MWCNT content. This corresponds to the laser ablation damage region in front of the notch tip [29]. The crack length used in the calculation of K_{Ic} is easily identified as the notch length (region A) plus the length of the microcracked damaged zone (region B) clearly observed on the fracture surface. The effective length of the crack was taken as the length of the notch plus the length of region B where the damage was observed. Therefore, the different appearance of region B is associated, in the current study, to the coalescence of the

damage induced by laser ablation in front of the notch during fracture. The damage is restricted to the length of region B and to a maximum average depth of 2 μm below the fracture surface. This can be appreciated in **Fig. 8~~6~~** where sections of region B (**Fig. 8~~6~~a**) and of the border between regions B and C (**Fig. 8~~6~~b**) are shown. On the left (region B) microcracking and porosity can be observed below the surface while just to the right in region C no trace of microcracking is observed. Similar observations using a notch tip induced by UPLA in conventionally sintered 3Y-TZP have been observed [29].

The true K_{Ic} values of the notched ~~S~~specimens using UPLA are given in **Table 1,** where it can be appreciated that K_{IC} values hardly change with the addition of MWCNT content. Moreover, the true K_{Ic} of monolithic SPSed 3Y-TZP is found to be smaller ($K_{Ic=}2.7$ MPam$^{1/2}$) than the conventionally sintered monolithic 3Y-TZP of larger grain size (~330 nm) where a K_{Ic} slightly higher than 4 MPam$^{1/2}$ was reported previously by the present authors [29].

It is interesting to notice that the higher values of K_{Ic} reported in the literature using the standard SEVNB method for the same composites include also a high K_{Ic} value for the starting monolithic 3Y-TZP matrix of about 6 MPa MPam$^{1/2}$ [20]. It should be noticed that this is a very high value for 3Y-TZP with a grain size of 145 nm. Since the starting powder, grain size and density of SPS 3Y-TZP reported in [20] are very similar to the present study, the difference regarding the K_{Ic} reported here could be associated to the sharpness of the starting notches. The present low K_{Ic} for 177 nm grain size 3Y-TZP (2.7 MPam$^{1/2}$) is in line with the results of Eichler et *al.*[33] where they reported values between 2.8 and 3.1 MPam$^{1/2}$ for 3Y-TZP with grain sizes in the range between 110 and 210 nm. Therefore, it may be concluded that at least part of the low K_{Ic} values measured

for the composites with respect to [20] is related to the matrix and possibly to the sharpness of the notch and length of microcracks induced in front of the notch.

As is shown above, here the damage in the form of microcracks in front of the notch is clearly revealed on the fracture surface. It is much longer than the notch radius, and it ends abruptly at some distance of the notch tip. This is the reason for taking the length of the initial crack as the length of the notch plus the length of the microcracked zone as it has been shown in [29]. If only the notch length was considered as the crack length, then even much lower values of K_{Ic} would be found. On the other hand, it is unlikely that the low value of K_{Ic} is related to the short depth of the shallow starting notch since the R-curve in nano grain size 3Y-TZP is relatively weak and very steep [33].

As seen in **Table 1**, the true K_{Ic} does not practically increase with MWCNT content. However, the contact damage resistance measured by indentation K_{Ic} increases. There were slight differences in the morphology of the crack paths with the addition of MWCNTs. However, the crack lengths are small and do not contribute significantly to the indentation fracture toughness. We rather associate the enhanced contact-damage resistance related to a reduction in the driving force for indentation crack growth related to change in plastic deformation behavior below the indentation. The intense confined-shear under Vickers indentation in the presence of shear-deformable MWCNTs in the small agglomerates increases irreversible deformation by this mechanism as well as by compaction of porosity below the indenter instead of by plastic deformation. The reason for this behaviour is probably related to the weak interfacial bonding between MWCNTs and zirconia matrix.

Damage

No fracture events like radial cracks at the corners of the imprints were detected ~~No damage events slip lines or transformations were observed just~~ under the Berkovich indentations (see **Fig.9~~7~~**). This indicates that the presence of fine grain microstructure (see **Fig.3~~2~~**) improves the damage tolerance under contact loading and it blocks the deformation mechanisms induced during the indentation process, which is similar to the behaviour reported in particle-dispersion-toughening of ceramic based nanocomposites [34].

The amount of *t-m* phase transformation below the indenter has not been measured in the present study. It was reported in a previous work [6], that *t-m* transformation is reduced in 3YTZP/CNT composites because of the small grain size. With the addition of 2 vol% MWCNT with grain size similar to the present study, *t-m* transformation at the fracture plane of Vickers indentation cracks was less than 5% at distances less than ≈ 2.0 μm below the fracture surface. Therefore less transformation would be expected below the indenter since the main stress state is compression.

4. Conclusions

True K_{Ic} of spark plasma sintered 3Y-TZP/CNT composites was successfully calculated using a novel method based on inducing a very sharp notch by UPLA. The true K_{Ic} for the SPSed 3Y-TZP matrix studied is smaller as compared to presureless conventional sintered 3Y-TZP. Moreover, the true K_{Ic} hardly increases with the addition of MWCNT while the indentation K_{Ic} of the starting 3Y-TZP matrix is higher and it increases with MWCNTs content.

It is concluded that the resistance to indentation cracking of the composites by adding MWCNTs to 3Y-TZP matrix does not indicate higher true fracture toughness. It is suggested that this is related to the drop in hardness and elastic modulus with the addition of MWCNTs content as it was detected using Berkovich nanoindentation.

Acknowledgements

The authors gratefully acknowledge the financial support given by the "Ministerio de Economía ~~Ciencia~~ y Competitividad" of Spain through research grant MAT2011-23913. L. M. acknowledges the fellowship received from the Joint Doctoral Programme in Materials Science and Engineering (DocMASE). All authors thank Dr. T. Trifonov and Dr. E. Jiménez for their assistance in the FIB/SEM equipment and nanoindenter, respectively.

References

[1] J. Chevalier, L. Gremillard, A. V. Virkar, D.R. Clarke, The Tetragonal-Monoclinic Transformation in Zirconia: Lessons Learned and Future Trends, J. Am. Ceram. Soc. 92 (2009) 1901–1920.

[2] R. Chintapalli, A. Mestra, F. García Marro, H. Yan, M. Reece, M. Anglada, Stability of Nanocrystalline Spark Plasma Sintered 3Y-TZP, Materials (Basel). 3 (2010) 800–814.

[3] E. Zapata-Solvas, D. Gómez-García, A. Domínguez-Rodríguez, Towards physical properties tailoring of carbon nanotubes-reinforced ceramic matrix composites, J. Eur. Ceram. Soc. 32 (2012) 3001–3020.

[4] G.-D. Zhan, J.D. Kuntz, J. Wan, A.K. Mukherjee, Single-wall carbon nanotubes as attractive toughening agents in alumina-based nanocomposites., Nat. Mater. 2 (2003) 38–42.

[5] X. Wang, N.P. Padture, H. Tanaka, Contact-damage-resistant ceramic/single-wall carbon nanotubes and ceramic/graphite composites., Nat. Mater. 3 (2004) 539–44.

[6] R.K. Chintapalli, F.G. Marro, B. Milsom, M. Reece, M. Anglada, Processing and characterization of high-density zirconia-carbon nanotube composites, Mater. Sci. Eng. A. (2012).

[7] M. Mazaheri, D. Mari, R. Schaller, G. Bonnefont, G. Fantozzi, Processing of yttria stabilized zirconia reinforced with multi-walled carbon nanotubes with attractive mechanical properties, J. Eur. Ceram. Soc. 31 (2011) 2691–2698.

[8] N. Garmendia, I. Santacruz, R. Moreno, I. Obieta, Slip casting of nanozirconia/MWCNT composites using a heterocoagulation process, J. Eur. Ceram. Soc. 29 (2009) 1939–1945.

[9] A. Datye, K.-H. Wu, G. Gomes, V. Monroy, H.-T. Lin, J. Vleugels, et al., Synthesis, microstructure and mechanical properties of Yttria Stabilized Zirconia (3YTZP) – Multi-Walled Nanotube (MWNTs) nanocomposite by direct in-situ growth of MWNTs on Zirconia particles, Compos. Sci. Technol. 70 (2010) 2086–2092.

[10] J.-H. Shin, S.-H. Hong, Microstructure and mechanical properties of single wall carbon nanotube reinforced yttria stabilized zircona ceramics, Mater. Sci. Eng. A. 556 (2012) 382–387.

[11] J.P. Zhou, Q.M. Gong, K.Y. Yuan, J.J. Wu, Y.F. Chen, C.S. Li, et al., The effects of multiwalled carbon nanotubes on the hot-pressed 3mol% yttria stabilized zirconia ceramics, Mater. Sci. Eng. A. 520 (2009) 153–157.

[12] J. Yi, T. Wang, Z. Xie, W. Xue, Zirconia-based nanocomposite toughened by functionalized multi-wall carbon nanotubes, J. Alloys Compd. 581 (2013) 452–458.

[13] T. Ukai, T. Sekino, A.T. Hirvonen, N. Tanaka, T. Kusunose, T. Nakayama, et al., Preparation and Electrical Properties of Carbon Nanotubes Dispersed Zirconia Nanocomposites, Key Eng. Mater. 317-318 (2006) 661–664.

[14] J. Sun, L. Gao, M. Iwasa, T. Nakayama, K. Niihara, Failure investigation of carbon nanotube/3Y-TZP nanocomposites, Ceram. Int. 31 (2005) 1131–1134.

[15] N. Garmendia, S. Grandjean, J. Chevalier, L. a. Diaz, R. Torrecillas, I. Obieta, Zirconia–multiwall carbon nanotubes dense nano-composites with an unusual balance between crack and ageing resistance, J. Eur. Ceram. Soc. 31 (2011) 1009–1014.

[16] A. Duszová, J. Dusza, K. Tomášek, G. Blugan, J. Kuebler, Microstructure and properties of carbon nanotube/zirconia composite, J. Eur. Ceram. Soc. 28 (2008) 1023–1027.

[17] P. Hvizdoš, V. Puchý, A. Duszová, J. Dusza, Tribological behavior of carbon nanofiber–zirconia composite, Scr. Mater. 63 (2010) 254–257.

[18] J. Dusza, G. Blugan, J. Morgiel, J. Kuebler, F. Inam, T. Peijs, et al., Hot pressed and spark plasma sintered zirconia/carbon nanofiber composites, J. Eur. Ceram. Soc. 29 (2009) 3177–3184.

[19] G.D. Quinn, R.C. Bradt, On the Vickers Indentation Fracture Toughness Test, J. Am. Ceram. Soc. 90 (2007) 673–680.

[20] M. Mazaheri, D. Mari, Z.R. Hesabi, R. Schaller, G. Fantozzi, Multi-walled carbon nanotube/nanostructured zirconia composites: Outstanding mechanical properties in a wide range of temperature, Compos. Sci. Technol. 71 (2011) 939–945.

[21] R. Damani, R. Gstrein, R. Danzer, Critical notch-root radius effect in SENB-S fracture toughness testing, J. Eur. Ceram. Soc. 16 (1996) 695–702.

[22] J. Kübler, FRACTURE TOUGHNESS OF CERAMICS USING THE SEVNB METHOD ; ROUND ROBIN.

[23] H. Fischer, A. Waindich, R. Telle, Influence of preparation of ceramic SEVNB specimens on fracture toughness testing results., Dent. Mater. 24 (2008) 618–22.

[24] B. Milsom, G. Viola, Z. Gao, F. Inam, T. Peijs, M.J. Reece, The effect of carbon nanotubes on the sintering behaviour of zirconia, J. Eur. Ceram. Soc. 32 (2012) 4149–4156.

[25] K. Niihara, A fracture mechanics analysis of indentation-induced Palmqvist crack in ceramics, J. Mater. Sci. Lett. 2 (1983) 221–223.

[26] G.R. Anstis, P. Chantikul, B.R. Lawn, D.B. Marshall, A Critical Evaluation of Indentation Techniques for Measuring Fracture Toughness: I, Direct Crack Measurements, J. Am. Ceram. Soc. 64 (1981) 533–538.

[27] T. Fett, Estimated stress intensity factors for semi-elliptical cracks in front of narrow circular notches, Eng. Fract. Mech. 64 (1999) 357–362.

[28] D. Munz, T. Fett, Ceramics: Mechanical Properties, Failure Behaviour, Materials Selection, Springer, 1999.

[29] M. Turon-Viñas and M. Anglada, Fracture toughness of zirconia from a shallow notch produced by ultra-short pulsed laser ablation, J. Eur. Ceram. Soc. 34 (2014) 3865-3870.

[30] W.C. Oliver, G.M. Pharr, Measurement of hardness and elastic modulus by instrumented indentation: Advances in understanding and refinements to methodology, J. Mater. Res. 19 (2011) 3–20.

[31] I. Horcas, R. Fernández, J.M. Gómez-Rodríguez, J. Colchero, J. Gómez-Herrero, A.M. Baro, WSXM: a software for scanning probe microscopy and a tool for nanotechnology., Rev. Sci. Instrum. 78 (2007) 013705.

[32] C. Laurent, E. Flahaut, A. Peigney, The weight and density of carbon nanotubes versus the number of walls and diameter, Carbon N. Y. 48 (2010) 2994–2996.

[33] J. Eichler, J. Rödel, U. Eisele, M. Hoffman, Effect of Grain Size on Mechanical Properties of Submicrometer 3Y-TZP: Fracture Strength and Hydrothermal Degradation, J. Am. Ceram. Soc. 90 (2007) 2830–2836.

[34] H. Awaji, S.-M. Choi, E. Yagi, Mechanisms of toughening and strengthening in ceramic-based nanocomposites, Mech. Mater. 34 (2002) 411–422.

Table captions:

Table 1. Properties of the 3Y-TZP/CNT nanocomposites**.**

Figure captions:

Fig. 1. Fracture surface showing the presence of porosity in the composite with 2 wt% CNT content.

Fig. 2~~1~~. Fracture surfaces of the sintered nanocomposites; (a) 0.5 wt% CNT, (b) 1 wt% CNT, (c) 2 wt% CNT composites.

Fig.3~~2~~. Microstructure of (a) 0 wt% CNT, (b) 0.5 wt% CNT, (c) 1 wt% CNT, (d) 2 wt% CNT composites after etching in air at high temperature.

Fig. 4~~3~~. Berkovich hardness and elastic modulus of all composites in terms of penetration depth.

Fig. 5. View of the notch induced by UPLA on specimen with 0 wt% CNT content.

Fig. 6~~4~~. Fracture surface of notched specimens: (a) 0 wt% CNT, (b) 0.5 wt% CNT and (c) 2 wt% CNT composites. **A** is the surface of the notch, **B** the microcracked region in front of the notch and **C** is the final fracture.

Fig. 7~~5~~. High ~~M~~magnification of the transitions between regions **A**, **B** and **C**.

Fig. 8~~6~~. (a) FIB cross section of the fracture surface below region **B**: (b) fracture surface with a trench at the border of regions **B** and **C**. The border coincides with the disappearance of damage below the surface.

Fig. 97. AFM topography image (3D view, 20 x 20 μm2) of nanoindentation imprints performed at maximum penetration depth on (a) 0 wt. % CNT, (b) 0.5 wt. % CNT, (c) 1 wt. % CNT, (d) 2 wt. % CNT composites.

Table 1

Table 1. Properties of the 3Y-TZP/CNT nanocomposites

Specimen	Relative density (TD %)	Grain size (nm)	H (GPa)	H_{Berk} (GPa)	E_{Berk} (GPa)	KIc* (MPa√m)	KIc** (MPa√m)
3Y-TZP	99.4±0.2	177±14	14.21±0.09	20.0 ± 0.4	263 ± 5	3.57±0.09	**2.7±0.1**
3Y-TZP+0.5 wt.% CNT	99.2±0.3	176±10	12.98±0.08	15.9 ± 0.4	224 ± 4	4.02±0.05	**2.7±0.1**
3Y-TZP+1 wt.% CNT	98.2±0.3	161±11	11.32±0.10	15.9 ± 0.7	215 ± 7	4.56±0.08	**2.8±0.1**
3Y-TZP+2 wt.% CNT	97.4±0.2	148 ± 9	9.52±0.05	12.7 ± 0.7	181 ± 6	4.97±0.06	**2.8±0.1**

*Indentation method of Anstis et al. [26]

**SENB specimen with notch machined with UPLA

Figure 1

Click here to download high resolution image

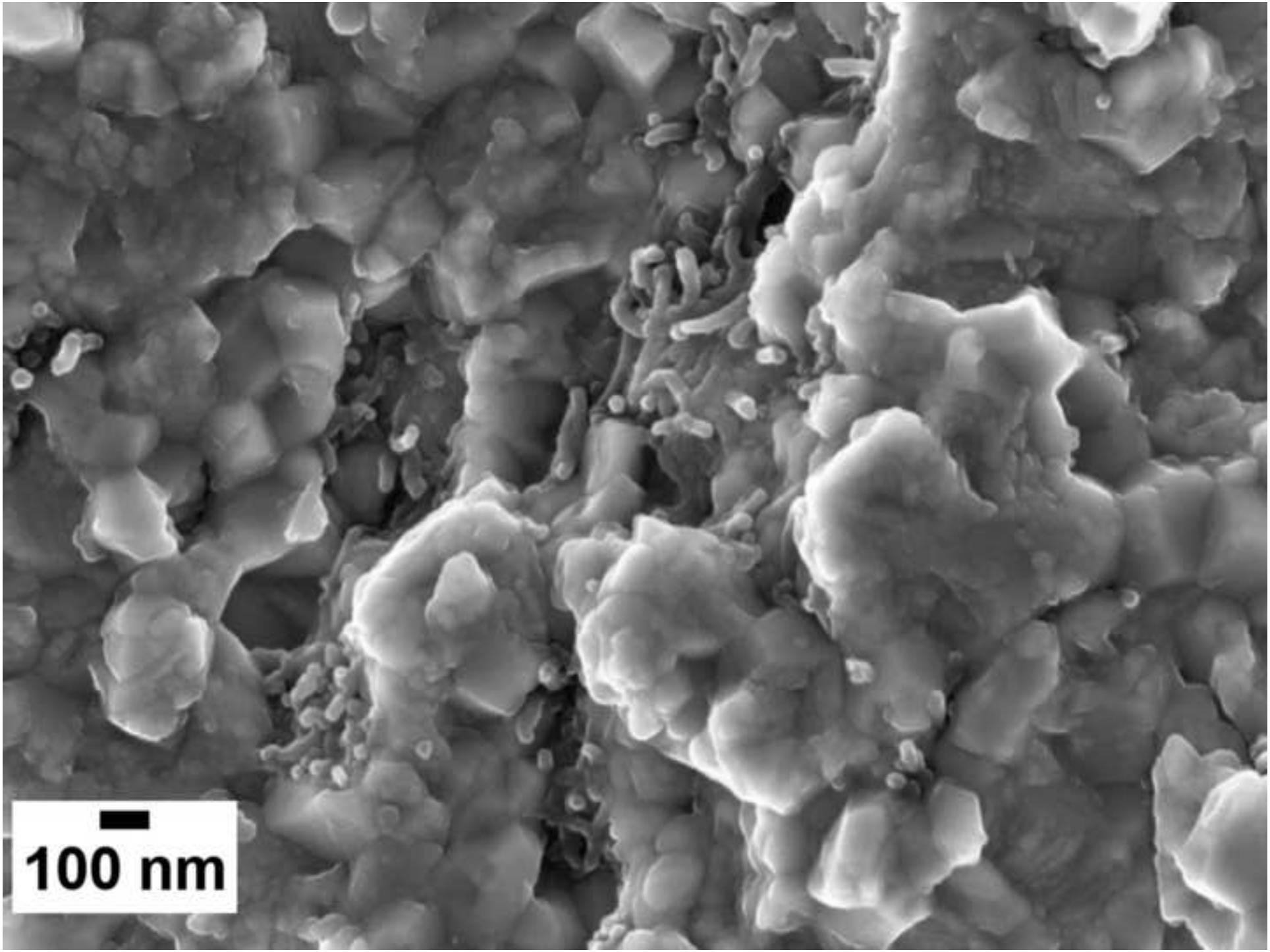

Figure 2

Click here to download high resolution image

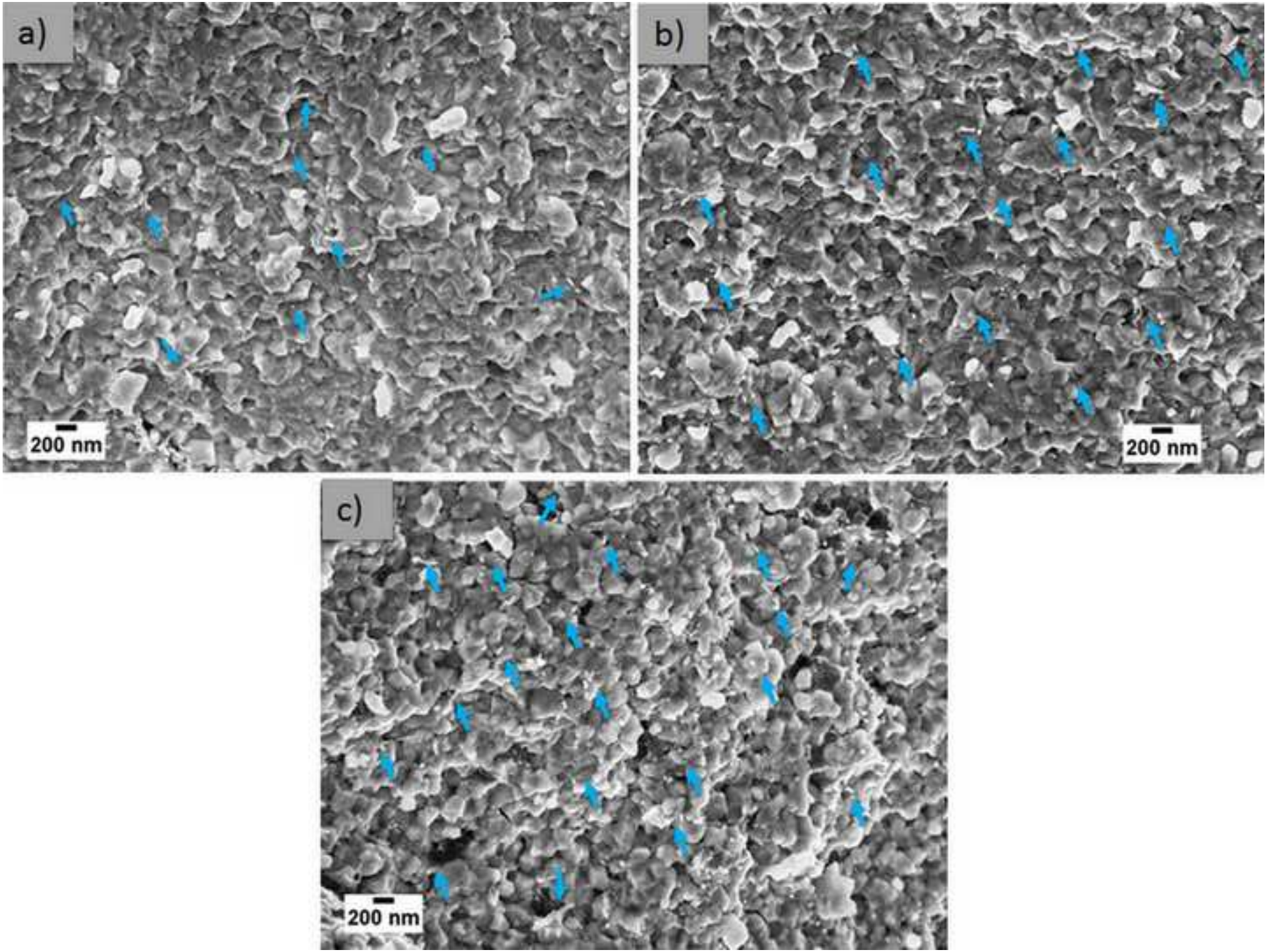

Figure 3

Click here to download high resolution image

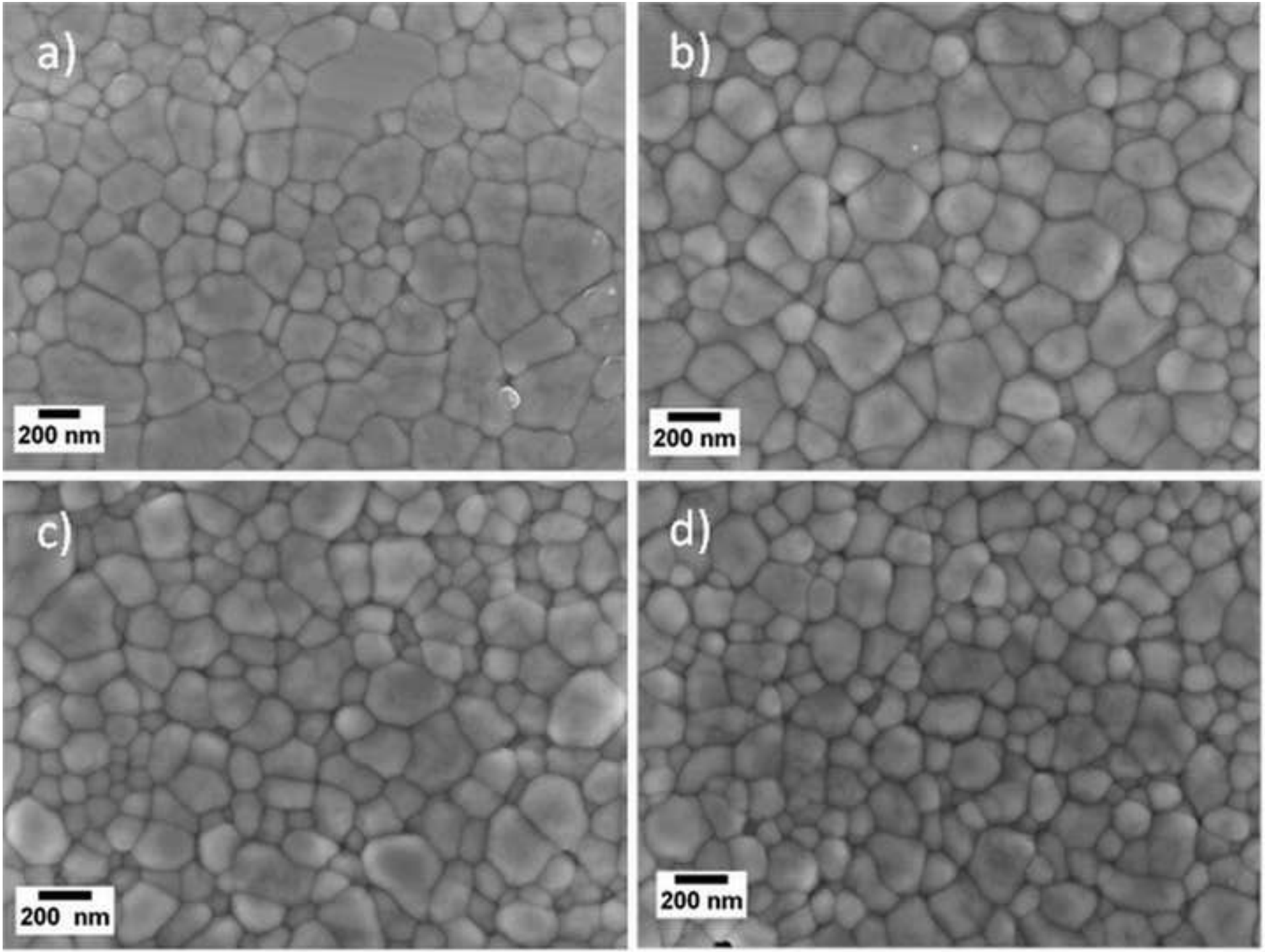

Figure 4

Click here to download high resolution image

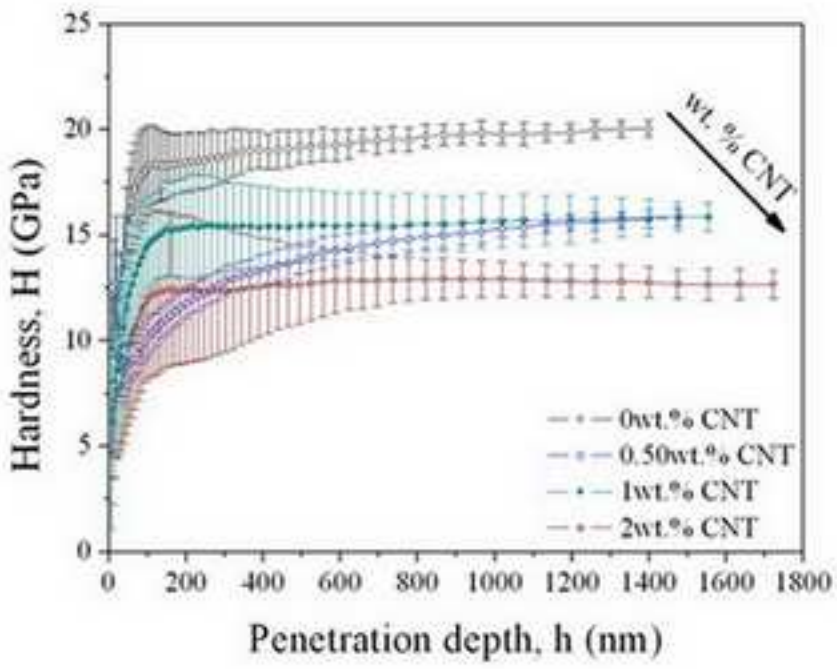

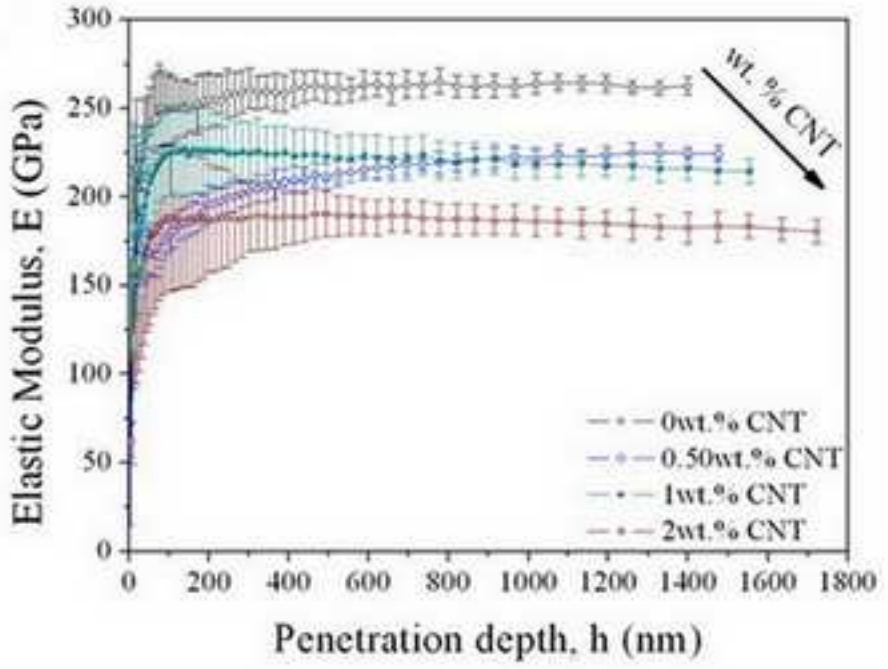

Figure 5

Click here to download high resolution image

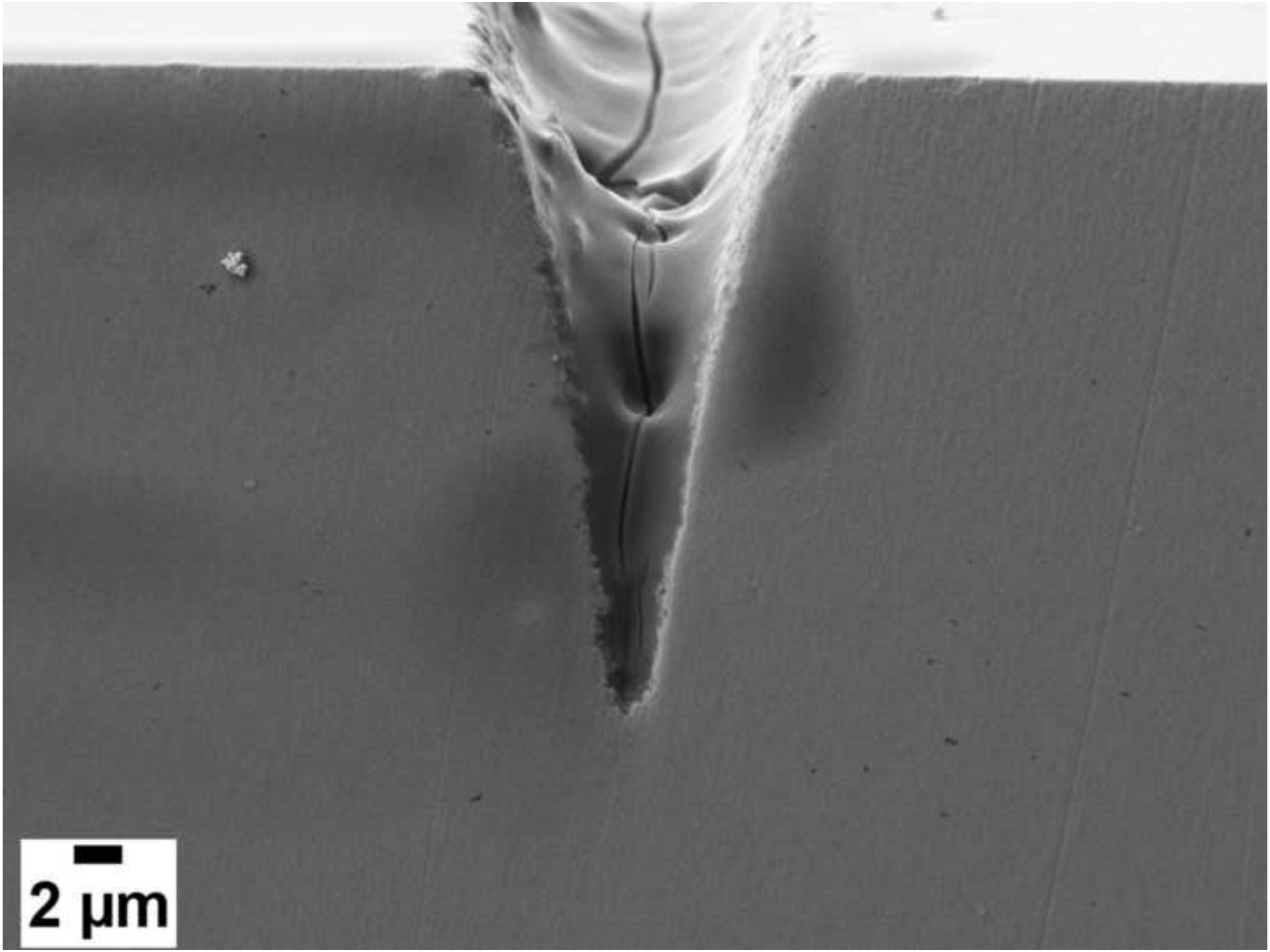

Figure 6

Click here to download high resolution image

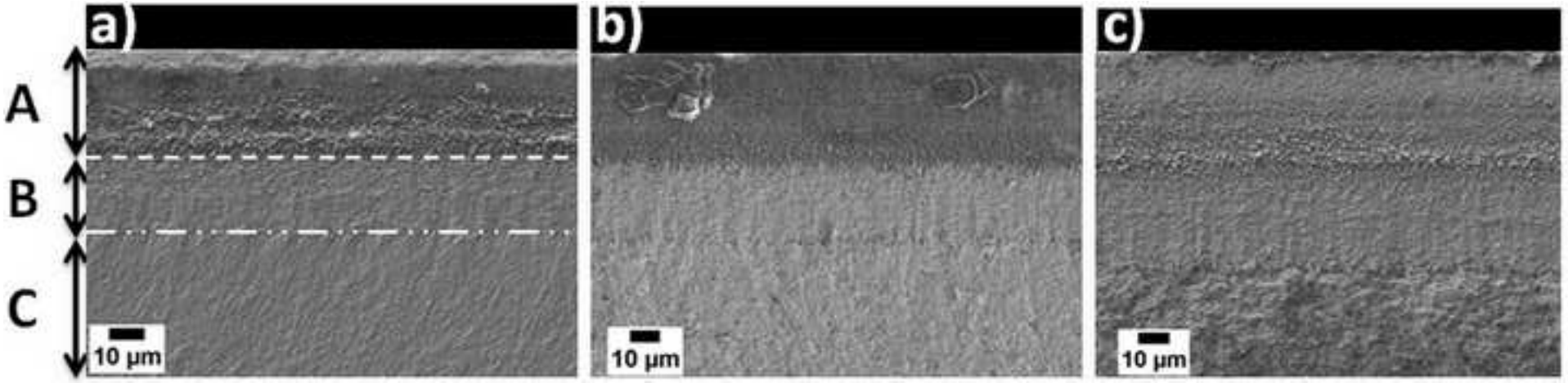

Figure 7

Click here to download high resolution image

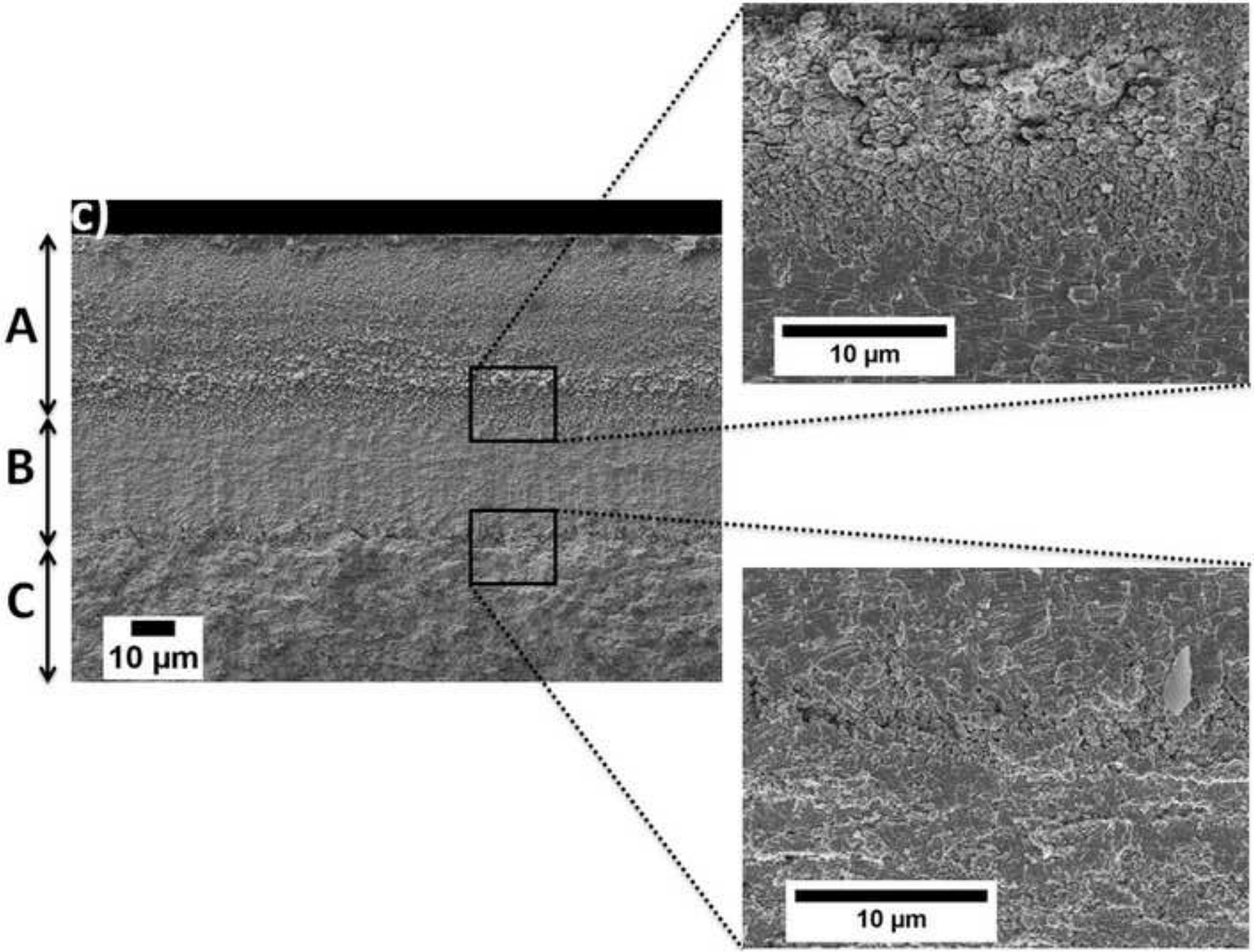

Figure 8
Click here to download high resolution image

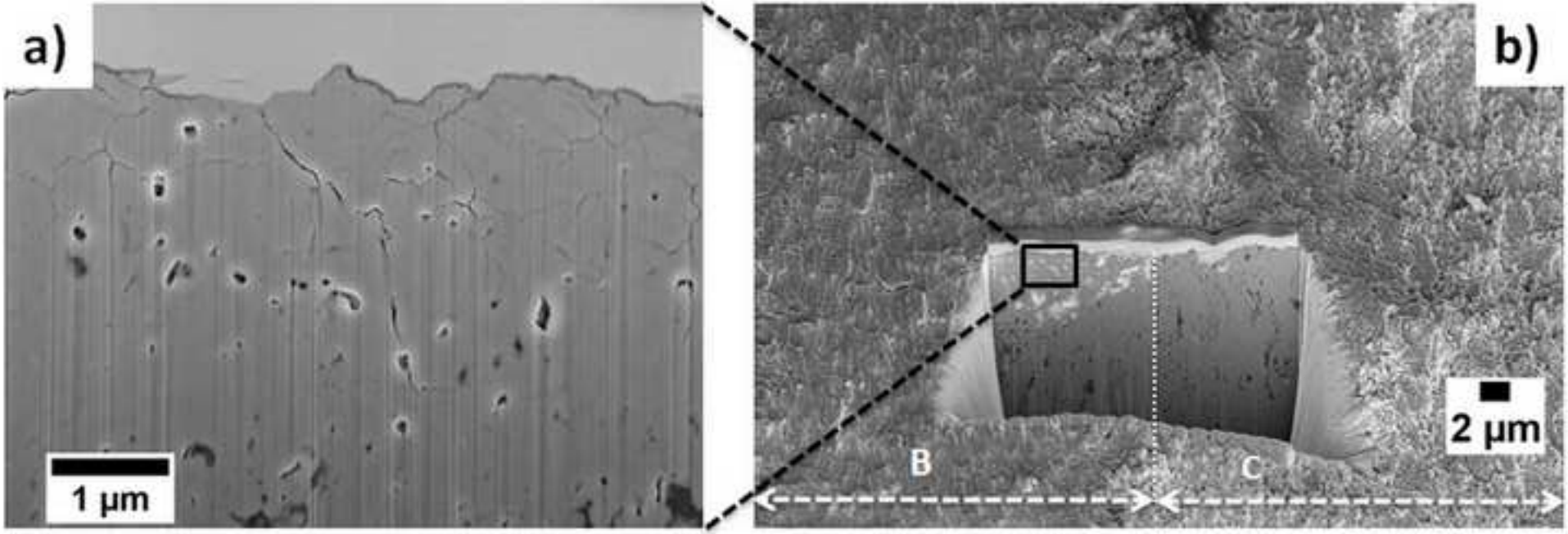

Figure 9

Click here to download high resolution image